Infrared vibrational photon echo experiments in liquids and glasses

ARTICLE *in* PROCEEDINGS OF SPIE - THE INTERNATIONAL SOCIETY FOR OPTICAL ENGINEERING · SEPTEMBER 1995

Impact Factor: 0.2 · DOI: 10.1021/j100036a003

FEATURE ARTICLE

Infrared Vibrational Photon Echo Experiments in Liquids and Glasses

A. Tokmakoff,† D. Zimdars, R. S. Urdahl, R. S. Francis, A. S. Kwok, and M. D. Fayer*

Department of Chemistry, Stanford University, Stanford, California 94305

Received: May 12, 1995®

The vibrational dynamics of polyatomic solutes in polyatomic liquid and glassy solvents are examined using picosecond infrared photon echo experiments and pump−probe experiments from room temperature to 10 K. The photon echo experiments measure T_2, the homogeneous dephasing time (homogeneous line shape), while the pump−probe experiments measure the vibrational lifetime, T_1, and the orientational relaxation dynamics. By combining these measurements, a complete analysis of vibrational dynamics is obtained in the liquid, in the supercooled liquid, through the glass transition, and in the glass. Experiments were conducted on the asymmetric CO stretching mode of tungsten hexacarbonyl (~1980 cm^{-1}) in 2-methylpentane (2-MP), 2-methyltetrahydrofuran, dibutyl phthalate (DBP), carbon tetrachloride, and chloroform. The experiments were conducted using the picosecond IR pulses from a superconducting-accelerator-pumped free electron laser. The absorption line widths for all glasses are massively inhomogeneously broadened at low temperature. In the room temperature liquids, while the vibrational line in 2-MP is homogeneously broadened, the line in DBP is still extensively inhomogeneously broadened. The temperature dependences of the homogeneous line widths in the three glasses are a T^2 power law. The contributions of vibrational pure dephasing, orientational relaxation, and population lifetime to the homogeneous line shape are examined in detail in the 2-MP solvent. The complete temperature dependence of each of the contributions is determined. In addition, the temperature dependence of T_1 is observed to be "inverted" in most of the solvents; i.e., the lifetime becomes longer as the temperature is increased. Analysis shows that this is caused by temperature dependence of the anharmonic coupling matrix elements.

I. Introduction

Vibrational spectra of even large molecules reveal detailed structure, a large number of lines that can be assigned to the various types of motions that occur in a molecule. The position of the spectroscopic peak associated with a particular mode yields the energy of the vibration. However, in general, even a well-resolved vibrational line does not provide information on dynamics. In principle, dynamical information is contained in a spectroscopic line shape. Vibrational line shapes in condensed phases contain all of the details of the interactions of a normal mode with its environment. These interactions include the important microscopic dynamics, intermolecular couplings, and involve the time scales of solvent evolution that modulate the energy of a transition. However, the line shape can also include essentially static structural perturbations associated with the distribution of local solvent configurations (inhomogeneous broadening). An infrared absorption spectrum or Raman spectrum gives frequency-domain information on the ensemble-averaged interactions that couple to the states involved in the transition.[1−3] Line shape analysis of vibrational transitions has long been recognized as a powerful tool for extracting information on molecular dynamics in condensed phases.[4,5] The difficulty with determining the microscopic dynamics from a spectrum arises because linear spectroscopic techniques have no method for separating the various contributions to the vibrational line shape. The IR absorption or Raman line shape represents a convolution of the various dynamic and static contributions to the observed line shape. In some cases, polarized Raman spectra can be used to separate orientational and vibrational dynamics from the line shape, yet as with all linear spectroscopies, contributions from inhomogeneous broadening cannot be eliminated.[6]

To completely understand a vibrational line shape, a series of experiments are required to characterize each of its static and dynamic components. These experiments can be effectively accomplished in the time domain, where well-defined techniques exist for measuring the various quantities. Nonlinear vibrational spectroscopy can be used to eliminate static inhomogeneous broadening from IR and Raman line shapes.[6] Techniques such as the infrared photon echo[7−9] and Raman echo[10−13] can determine the homogeneous vibrational line shape which contains the important microscopic dynamics, when this line shape is masked by inhomogeneous broadening.

Below we present the temperature-dependent vibrational dynamics of the triply degenerate T_{1u} CO stretching mode (~1980 cm^{-1}) of tungsten hexacarbonyl ($W(CO)_6$) in the molecular glass-forming liquids 2-methyltetrahydrofuran (2-MTHF), 2-methylpentane (2-MP), and dibutyl phthalate (DBP). Two aspects of the vibrational line shape in these systems are discussed in detail. Initially, we compare the behavior of the homogeneous line widths in the glasses and the transition to the room temperature liquids for the three solvents, using picosecond IR photon echo experiments. The temperature dependence of the vibrational dephasing and the degree of

* To whom correspondence should be addressed.
† Present address: Physik Department, Technische Universität München, D85748 Garching, Germany.
® Abstract published in *Advance ACS Abstracts*, August 15, 1995.

0022-3654/95/2099-13310$09.00/0

inhomogeneity as the liquids approach room temperature are discussed. The temperature dependence of the homogeneous vibrational line width in each of the three glassy solvents is T^2, but the behavior is distinct in each of the liquids. While in 2-MP the vibrational line is homogeneously broadened at room temperature, the line in DBP is massively inhomogeneously broadened in the room temperature liquid.

Following the comparison of the temperature-dependent dephasing in the three solvents, one of the systems, $W(CO)_6$ in 2-MP is analyzed in greater detail. The contributions to the vibrational line shape from different dynamic processes are delineated by combining the results of photon echo measurements of the homogeneous line shape[8] with pump−probe measurements of the lifetime and reorientational dynamics.[14] This combination of measurements allows the decomposition of the total homogeneous vibrational line shape into the individual components of pure dephasing (T_2*), population relaxation (T_1), and orientational relaxation. The results demonstrate that each of these can contribute significantly, but to varying degrees at different temperatures.

In measuring T_1, it was found that in a number of solvents the lifetimes become longer as the temperature is increased.[14-17] This counterintuitive temperature dependence is examined more closely in the solvents carbon tetrachloride (CCl_4) and chloroform ($CHCl_3$).[17] Analysis of the influence of the temperature dependence of the occupation numbers of the solute and solvent modes[16,18] and of the solvent density of states[16] shows that these cannot account for the "inverted" temperature dependence. This suggests that the temperature dependence of the liquid density, resulting in changes in the anharmonic potential, is responsible for the form of the temperature dependence.[16]

II. Infrared Vibrational Photon Echo Experiments

A. The Nature of the Experiment. The picosecond infrared vibrational photon echo experiment is a time domain nonlinear experiment that can extract the homogeneous vibrational line shape even when the inhomogeneous line width is thousands of times wider than the homogeneous width. The echo technique was originally developed as the spin echo in magnetic resonance in 1950.[19] In 1964, the method was extended to the optical regime as the photon echo.[20] Since then, photon echoes have been used extensively to study electronic excited state dynamics in many condensed matter systems. For experiments on vibrations, a source of picosecond IR pulses is tuned to the vibrational transition of interest. The echo experiment involves a two-pulse excitation sequence. The first pulse puts the solutes' vibrations into superposition states, which are mixtures of the $v = 0$ and $v = 1$ vibrational levels. Each superposition has a microscopic electric dipole associated with it. This dipole oscillates at the vibrational transition frequency. Immediately after the first pulse, all of the microscopic dipoles in the sample oscillate in phase. Because there is an inhomogeneous distribution of vibrational transition frequencies, the individual dipoles oscillate with some distribution of frequencies. Thus, the initial phase relationship is very rapidly lost. This is referred to as the free induction decay. After a time, τ, a second pulse traveling along a path making an angle θ with that of the first pulse passes through the sample. This second pulse changes the phase factors of each vibrational superposition state in a manner that initiates a rephasing process. At time τ after the second pulse, the sample emits a third coherent pulse of light along a unique path which makes an angle 2θ with the direction of the first pulse (see Figure 1a). The third pulse is the photon echo. It is generated when the ensemble of microscopic dipoles are rephased at time 2τ. The phased array of microscopic

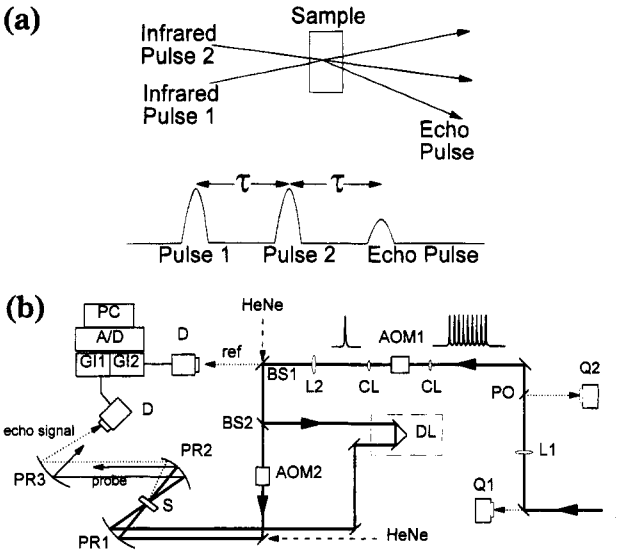

Figure 1. (a) Schematic diagram of the infrared vibrational photon echo experiment. Two picosecond IR pulses tuned to the vibrational transition frequency enter the sample crossed at a small angle, θ. Because of wave vector matching, the echo pulse emerges from the sample in a unique direction, 2θ. Pulse 1 and pulse 2 are separated by time τ. The echo is formed a time 2τ after pulse 1. (b) Experimental apparatus. Pulse selection is accomplished with AOM1, while AOM2 is used for chopping of pulse 2. Abbreviations: AOM, acoustooptic modulator; A/D, analog-to-digital converter; BS, ZnSe beam splitter; CL, cylinderical lens; D, detector; DL, optical delay line; GI, gated integrator; L, lens; PC, personal computer; PO, pick-off; PR, off-axis parabolic reflector; Q, position-sensitive detector; S, sample.

dipoles behaves as a macroscopic oscillating dipole, which generates an IR pulse of light. A free induction decay (inhomogeneous frequency distribution) again destroys the phase relationships, so only a short pulse of light is generated.

The rephasing at 2τ has removed the effects of the inhomogeneous broadening. However, fluctuations due to coupling of the vibrational mode to the heat bath (solvent) cause the oscillation frequencies to fluctuate. Thus, at 2τ there is not perfect rephasing. As τ is increased, the fluctuations produce an increasingly large accumulated phase error, and the size of the echo is reduced. A measurement of the echo intensity vs τ, the delay time between the pulses, is called an echo decay curve. Thus, the echo decay is related to the fluctuations in the vibrational frequencies, not the inhomogeneous spread in frequencies. The Fourier transform of the echo decay is the homogeneous line shape.[21] For example, if the echo decay is an exponential, the line shape is a Lorentzian with a width $1/\pi T_2$ determined by the exponential decay constant. The vibrational photon echo makes the vibrational homogeneous line shape an experimental observable. In fact, the echo measures directly the decay of the system's off-diagonal density matrix elements and is the most fundamental observable.

B. Correlation Function Description of the Vibrational Line Shape. For a dilute solution of a vibrational chromophore, the homogeneous vibrational line width, Γ, generally has contributions from the rate of population relaxation (lifetime), $1/T_1$, the rate of pure dephasing, $1/T_2$*, and the rate of orientational relaxation, Γ_{or}. T_1 processes are caused by the anharmonic coupling of the vibrational mode to the bath. The bath includes other vibrational modes of the solute and the solvent and the low-frequency continuum of intermolecular solvent modes.[17,18,22,23] Population relaxation is the only dynamic process that can contribute to the vibrational line width in the limit that $T \rightarrow 0$ K.[18,24] Pure dephasing describes the adiabatic modulation of the vibrational energy levels of a

transition caused by thermal fluctuations of its environment.[25,26] Measurement of this quantity provides detailed insight into the fast dynamics of the system. Although generally equated with physical rotation of the dipole, orientational relaxation is defined as any process that causes the loss of angular correlation of an ensemble of dipoles. For the T_{1u} mode of $W(CO)_6$ studied here, orientational relaxation occurs through the time evolution of the coefficients of the three states in the superposition created by the initial excitation of the triply degenerate T_{1u} mode.[14,15] Both pure dephasing and orientational relaxation will vanish in the limit that $T \rightarrow 0$ K, since they are thermally induced processes.

The infrared absorption line shape is related to these microscopic dynamics through the Fourier transform of the two-time transition dipole correlation function[1-3,26]

$$I(\omega) = (2\pi)^{-1} \int_{-\infty}^{+\infty} dt\, e^{i\omega t} \langle \mu(t) \cdot \mu^*(0) \rangle \quad (1)$$

The infrared absorption spectrum gives dynamic information on $\langle P_1(\mu(t)\cdot\mu^*(0))\rangle$, where P_1 is the first Legendre polynomial. If the vibrational and rotational motions are decoupled, then the dipole correlation function can be factored

$$\langle \mu(t) \cdot \mu^*(0) \rangle = \langle \mu(t)\, \mu^*(0) \rangle \langle \hat{\mu}(t) \cdot \hat{\mu}(0) \rangle \quad (2)$$

The first term in eq 2 describes the time dependence of the vibrational motions and is often written as[35]

$$\langle \mu(t)\, \mu^*(0) \rangle = |\mu|^2 \langle \exp[-i \int_0^t dt'\, \Delta(t')] \rangle \quad (3)$$

Here Δ describes the variations in the transition energies for the ensemble of vibration transition dipoles and includes any inhomogeneous broadening.[27] The second term in eq 2 is the ensemble-averaged correlation function for unit vectors along the dipole direction and describes the orientational motion of the dipole.

In the Markovian limit, in which these quantities are described by independent exponentially relaxing dipole correlation functions, the total transition dipole correlation function described by eq 2 decays exponentially at a rate of $1/T_2$, where T_2 is the dephasing time. This gives a Lorentzian line shape, and contributions to the full line width at half-maximum (fwhm) are additive

$$\Gamma = 1/\pi T_2 = 1/\pi T_2^* + 1/2\pi T_1 + \Gamma_{or} \quad (4)$$

The orientational contribution to the infrared line shape due to isotropic rotational diffusion of the dipole is determined by $\langle P_1(\hat{\mu}(t)\cdot\hat{\mu}(0))\rangle$ and,

$$\Gamma_{or} = 2D_{or}/\pi \quad (5)$$

where D_{or} is the orientational diffusion constant.[15,28] Equation 4 allows the contribution of pure dephasing to the vibrational line shape to be determined from a knowledge of the homogeneous line width, the vibrational lifetime, and the orientational diffusion constant.

C. The Infrared Photon Echo Experiment. The infrared photon echo[7-9] is a time-domain nonlinear technique that allows inhomogeneity to be removed from the vibrational line shape. The two-pulse photon echo, and other line narrowing techniques such as the stimulated photon echo and hole burning, eliminate the inhomogeneous contribution to the line shape and are described by four-time correlation functions[6] of the form

$$C = \langle \mu^*(t_3+t_2+t_1)\, \mu(t_2+t_1)\, \mu(t_1)\, \mu^*(0) \rangle \quad (6)$$

where t_1, t_2, and t_3 refer to three consecutive time intervals. We have written this form[29] of the correlation function for direct comparison to eq 1. The two-pulse photon echo is a third-order nonlinear experiment that uses three input fields E_i resonant with a vibrational transition to generate an output echo signal described by $C(t_3,t_2,t_1)$. The first field interaction is during the first pulse, and the second and third interactions are with the second pulse. For a delta function pulses with separation τ, the experiment is described by correlation functions of the form $\langle \mu^*(2\tau)\cdot\mu(\tau)\cdot\mu(\tau)\cdot\mu^*(0)\rangle$.

As with the two-time correlation function, the assumption that vibrational and rotational degrees of freedom are independent allows the four-time correlation function C to be separated as $C = C_v C_{or}$. The vibrational contribution to the four-time correlation function C_v is given by[6,30,31]

$$C_v(2\tau,\tau,\tau) = |\mu|^4 \langle \exp[i \int_\tau^{2\tau} dt'\, \Delta(t') - i \int_0^\tau dt'\, \Delta(t')] \rangle \quad (7)$$

Unlike eq 3, eq 7 allows for time reversal processes to remove inhomogeneity. If the Δ's in eq 7 are strictly static energies (inhomogeneous broadening only), then the two integrals are identical and cancel. Thus, inhomogeneous broadening does not contribute to the echo decay. Random, homogeneous energy fluctuations will not be identical in the two time intervals $0 \rightarrow \tau$ and $\tau \rightarrow 2\tau$. Therefore, the two integrals will not cancel identically, and homogeneous dephasing will contribute to the echo decay.

The contribution of orientational relaxation to the correlation function C_{or} can be written as

$$C_{or}(2\tau,\tau,\tau) = \langle \hat{\mu}(2\tau)\cdot\hat{\mu}(\tau)\cdot\hat{\mu}(\tau)\cdot\hat{\mu}(0) \rangle \quad (8)$$

which is the ensemble-averaged four-time correlation function for unit vectors along the transition dipole direction. C_{or} can be treated as a classical probability average when the orientational relaxation is diffusive.

The description of the third-order nonlinear polarization that governs infrared photon echo experiments in terms of the dynamics of lifetime, pure dephasing, and orientational diffusion has been presented.[15] For the case that the relaxation processes that contribute to the line shape are separable, the photon echo signal with delta function pulses decays exponentially as

$$I(\tau)/I(0) = \exp[-4\tau(1/T_2^* + 1/2T_1 + 2D_{or})] \quad (9a)$$

$$= \exp[-4\tau/T_2] \quad (9b)$$

The signal decays at a rate 4 times faster than the decay of the homogeneous dipole correlation function. The decay of the photon echo in this limit can be written as proportional to $|\langle \mu(\tau)\cdot\mu^*(0)\rangle|^4$ and thus gives the homogeneous vibrational line shape through eq 1. It is important to note that due to the separability of the rotational and vibrational degrees of freedom and the Markovian form of the correlation function decay, the four-time correlation function can be written as the product of two-time correlation functions.

D. Experimental Procedures. Vibrational photon echo experiments require tunable IR pulses with durations of ~1 ps and energies of ~1 μJ. These can be produced with systems based on conventional picosecond lasers using an optical parametric amplifier (frequency difference mixing) to generate the IR pulses. However, the experiments described below were performed using a different approach, i.e., with infrared pulses at ~5 μm generated by the Stanford superconducting-accelerator-pumped free electron laser (FEL). The FEL generates

Gaussian pulses that are transform limited with pulse duration that is adjustable between 0.7 and 2 ps. Active frequency stabilization allows wavelength drifts to be limited to <0.01% or <0.2 cm^{-1}. The pulse length and spectrum are monitored continuously with an autocorrelator and grating monochromator.

The FEL emits a 2 ms macropulse at a 10 Hz repetition rate. Each macropulse consists of the picosecond micropulses at a repetition rate of 11.8 MHz (84 ns). The micropulse energy at the input to experimental optics is ~0.5 μJ, and the corresponding energy in the full FEL beam is 120 mW. In vibrational experiments, virtually all power absorbed by the sample is deposited as heat. To avoid sample heating problems, micropulses are selected out of the macropulse at a reduced frequency.

The experimental apparatus is shown in Figure 1b. The infrared beam enters the experimental area roughly collimated with a 16 mm diameter. A 1:6× telescope (L1, L2) reduces the beam size. At the focus of the telescope is a Ge acoustooptic modulator (AOM) for pulse selection, within a 1:1 cylindrical telescope using CaF_2 lenses. Micropulses are selected out of each macropulse at a repetition rate of 50 kHz by the AOM single-pulse selector. The cylindrical telescope makes the AOM rise time less than the interpulse separation. This pulse selection yields an effective experimental repetition rate of 1 kHz and an average power of <0.5 mW. A ZnSe beam splitter allows 1% of the IR beam to be directed into a HgCdTe reference detector. The reference detector was used for shot intensity windowing; all data from pulses with intensities outside of a 10% window were discarded.

The two pulses for photon echo or pump−probe (transient absorption to measure the vibrational lifetime) experiments were obtained with a 10% ZnSe beam splitter. The 10% beam (first pulse in echo sequence and probe pulse) is sent through a computer-controlled stepper motor delay line. The remaining portion (second echo pulse or pump pulse) is chopped at 25 kHz by a second Ge AOM. A HeNe beam is made collinear with each IR beam for alignment purposes. The two pulses were focused in the sample to 220 μm diameter using an off-axis parabolic reflector for achromatic focusing of the IR and HeNe. The beams and echo signal were recollimated with a second parabolic reflector and focused into a HgCdTe signal detector with a third parabolic reflector. By selecting the desired beam with an iris between the second and third parabolic reflectors, either the photon echo or pump−probe signal could be observed. The photon echo signal and a intensity reference signal were sampled by two gated integrators and digitized for collection by computer.

Careful studies of power dependence and repetition rate dependence of the data were performed. It was determined that there were no heating or other unwanted effects when data were taken with pulse energies of ~15 nJ for the first pulse and ~80 nJ for the second pulse and the effective repetition rate of 1 kHz (50 kHz during each macropulse).

Vibrational photon echo and pump−probe data were taken on the triply degenerate T_{1u} asymmetric CO stretching mode of $W(CO)_6$. Solutions of $W(CO)_6$ in the glass-forming liquids were made to give a peak optical density of 0.8 with thin path length. These solutions correspond to mole fractions of $\leq 10^{-4}$. The temperatures of the samples were controlled to ±0.2 K using a closed-cycled He refrigerator.

Pump−probe experiments conducted in the solvents CCl_4 and $CHCl_3$ were performed with the 1 kHz output of an optical parametric amplifier using doubled YAG and a dye laser as inputs. This system has been described in detail.[32]

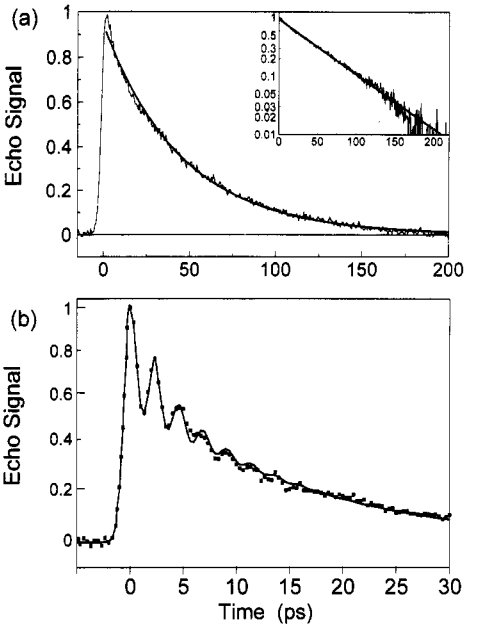

Figure 2. (a) Photon echo decay data for the CO asymmetric stretching mode (T_{1u}) of $W(CO)_6$ in 2-methylpentane glass at 10 K. The homogeneous line width determined by the echo decay is 1.3 GHz (0.04 cm^{-1}) in contrast to the absorption line which is inhomogeneously broadened to 310 GHz (10.5 cm^{-1}). (b) Vibrational photon echo decay and fit for asymmetric CO stretching mode of $W(CO)_6$ in dibutyl phthalate in the glass at 10 K. The fit is to eq 10 and represents the homogeneous dephasing of the three-level coherence with beating at the anharmonic vibrational frequency splitting.

III. Experimental Results

A. Vibrational Photon Echo Decays. Figure 2a displays photon echo data for $W(CO)_6$ in 2-MP taken in the low-temperature glass at 10 K.[8,15] The inset shows a log plot of the data. The decay is exponential, indicating that the homogeneous line is a Lorentzian. At this temperature, the absorption line width is 10.5 cm^{-1} (310 GHz). In contrast, $T_2 = 240$ ps, yielding a homogeneous line width of 1.3 GHz. Thus, the absorption line is massively inhomogeneously broadened.

Figure 2b displays data taken using 0.7 ps pulses in the solvent DBP.[9] When the pulse duration is made shorter, the associated bandwidth, Ω, of the transform limited pulse is larger. If the bandwidth of the excitation pulses exceeds the vibrational anharmonicity, then population can be excited to higher vibrational levels. For the case where $\Delta \approx \Omega$, short pulse excitation will create a three-level coherence involving the $v = 0$, 1, and 2 vibrational levels. The expected photon echo signal can be described for an unequally spaced three-level system using a semiclassical perturbative treatment of the third-order nonlinear polarizability in the Bloch limit.[30,33] The three-level system is spaced by the frequencies ω_{10} and ω_{21}, where $\omega_{10} = \omega_{21} + \Delta$ and $\Delta \ll \omega_{10}$ and ω_{21}. The transition frequencies ω_{10} and ω_{21} lie within the bandwidth of the pulses. For a finite pulse bandwidth, where the E-field amplitude differs at ω_{10} and ω_{21}, the decay is given by[9]

$$I(\tau) = \exp(-2\gamma_{10}\tau)[E_{10}^2 \exp(-2\gamma_{10}\tau) + E_{21}^2 \exp(-2\gamma_{21}\tau) - 2E_{10}E_{21} \exp(-(\gamma_{10} + \gamma_{21})\tau) \cos(\Delta\tau + \phi)] \quad (10)$$

Here, E_{10} and E_{21} are excitation E-field amplitudes for the $v = 0 \rightarrow 1$ and $v = 1 \rightarrow 2$ transitions, respectively. Equation 10 shows that the echo signal envelope decays in proportion to the dephasing rates of the $v = 0 \rightarrow 1$ and $v = 1 \rightarrow 2$ transitions,

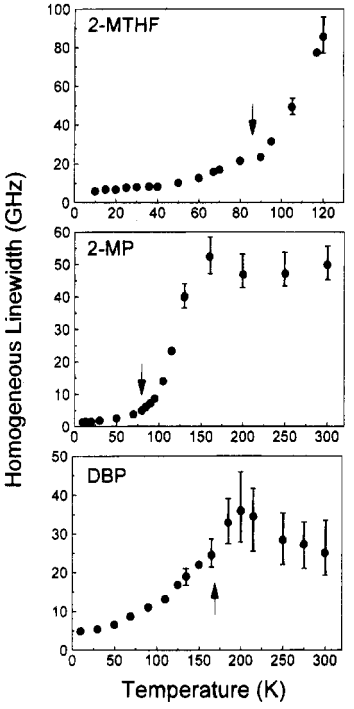

Figure 3. Temperature dependence of the homogeneous line widths of the T_{1u} CO stretching mode of $W(CO)_6$ in 2-MTHF, 2-MP, and DBP, determined from infrared photon echo experiments using eq 9b. Arrows mark the glass transition temperatures. Note the different temperature and line width scales.

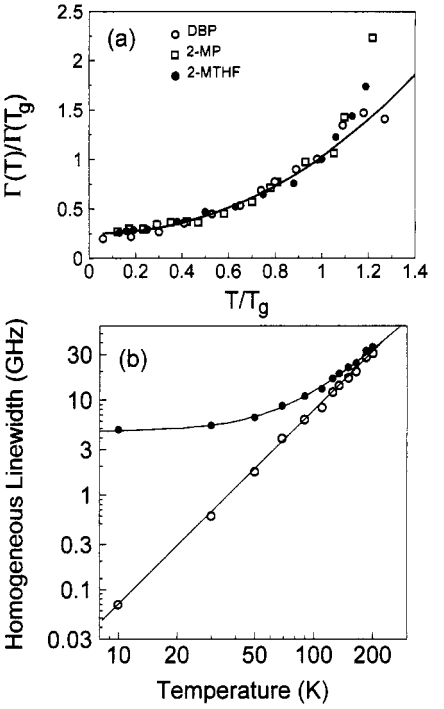

Figure 4. (a) Comparison of the homogeneous infrared line width in three organic glasses. The homogeneous line width normalized to the line width at the glass transition temperature to remove the coupling strength is plotted against the reduced temperature. The temperature dependence follows a power law with exponent $\alpha = 2.1 \pm 0.2$. (b) Homogeneous line width of the T_{1u} mode of $W(CO)_6$ in DBP between 10 and 200 K. The homogeneous line widths are shown in solid circles, and the corresponding data with the low-temperature lifetime of $T_1(0\ K) = 33$ ps removed are shown with open circles. The data fit a power law of $\alpha = 2.0 \pm 0.1$.

with exponentially damped beats observed at the frequency splitting, Δ. The dephasing rates for the two transitions are γ_{10} and γ_{21}. For the narrow bandwidth case ($E_{21} \approx 0$), eq 9b is recovered.

As can be seen from Figure 2b, the decay is consistent with the expected decay of a three-level vibrational coherence. The decay is modulated at a 2.3 ps frequency, which is constant within error over all temperatures. Based on the average of several data sets, the vibrational anharmonic splitting is $\Delta = 14.7 \pm 0.3\ cm^{-1}$.[9] This splitting is in accord with the value of $15 \pm 1\ cm^{-1}$ subsequently obtained by Heilweil and co-workers from observation of the $v = 1 \rightarrow 2$ and $v = 2 \rightarrow 3$ transitions of the asymmetric CO stretching mode of $W(CO)_6$ in hexane using transient infrared absorption.[34] The agreement between the anharmonicity obtained from the beat frequency and that obtained by transient absorption confirms the interpretation of the beats as arising from the multilevel coherence of the anharmonic oscillator. The echo decay data also provide the homogeneous dephasing times for the two transitions involved in the multilevel coherence.[9]

B. Temperature Dependence of Vibrational Dephasing. *1. Below the Glass Transition Temperature.* The results of temperature-dependent photon echo experiments on the T_{1u} mode of $W(CO)_6$ in the three glass-forming liquids[15] are shown in Figure 3. The homogeneous line width, $\Gamma = 1/\pi T_2$, is shown, derived from fits with the photon echo signal decaying exponentially as eq 9b. Data on 2-MTHF were taken from 10 to 120 K, at which point the decay rate exceeded the instrument response. With the same time resolution, echo data in the other liquids were observable up to room temperature. The data on DBP (discussed above) were taken with 0.7 ps pulses. At temperatures above 150 K, where the decays are fast, the presence of the beats on the decays introduced some uncertainty into the determination of the vibrational line width for the $v = 0 \rightarrow 1$ level.

The temperature dependence of the homogeneous line width increases monotonically in the glass. Above the glass transition temperature, the line widths in 2-MTHF ($T_g = 86$ K) and 2-MP ($T_g = 80$ K) rise rapidly in a manner that appears thermally activated. In 2-MP, the rapid increase in dephasing rate slows above 130 K and becomes temperature independent. In DBP ($T_g = 169$ K), the line width appears to decrease with temperature above 200 K although the error bars are large enough that it is possible that the temperature dependence is essentially flat.

The temperature dependences of the homogeneous vibrational line widths in the three glasses are compared using a reduced variable plot[15] in Figure 4a. Although the absolute line widths for each system may vary, this is a reflection of the strength of coupling of the transition dipole to the bath and can be removed by normalization to the line width at the glass transition temperature. Likewise, using a reduced temperature, T/T_g, allows thermodynamic variables that contribute to determining the glass transition to be normalized. Such normalization allows comparison of the functional form of the temperature dependences, independent of differences in T_g and coupling strengths. Figure 4a shows that the temperature dependences of the homogeneous line widths are identical in the three glasses and are well described by a power law of the form

$$\Gamma(T) = \Gamma_0 + AT^{\alpha} \tag{11}$$

The offset at 0 K, Γ_0, represents the line width due to the low-temperature vibrational lifetime. A fit to eq 11 for all temperatures below the glass transition is shown in Figure 4a and yields an exponent of $\alpha = 2.1 \pm 0.2$ and $\Gamma_0/\Gamma(T_g) = 0.24 \pm 0.02$. At temperatures above $\sim 1.2T_g$, the line widths of the

three liquids diverge from one another. The data from each sample were individually fit to eq 11. The results demonstrate that the temperature dependence is well described by a power law of the form T^2.

Because of its high glass transition temperature, DBP allows the largest temperature range over which to observe the power law. The data are presented in two ways in Figure 4b. The solid circles are the data and the line through them is a fit to eq 11. To show more clearly the power law temperature dependence, the open circles are the data with the low-temperature line width, Γ_0 (corresponding to a vibrational lifetime, $T_1(0\ K) = 33$ ps) subtracted out. The line through the data is T^2. It can be seen that the power law describes the data essentially perfectly over a change of line width of ~500 from 10 to 200 K.

Electronic excited state dephasing in glasses[35] is generally interpreted within the model of two-level systems, initially proposed to describe the anomalous low-temperature heat capacities of glasses.[36,37] In this model, pure dephasing dynamics are described in terms of phonon-induced tunneling between structural potential wells. At temperatures above the Debye frequency of the glass, a power law of T^2 is theoretically predicted for dephasing due to two-phonon (Raman) scattering processes between potential wells.[35] Huber has pointed out that in glasses this temperature dependence is expected above an effective Debye temperature, which can often be 2−10 times lower than the true Debye temperature.[38] The $\alpha \approx 2$ temperature dependence is almost universally seen for the high-temperature dephasing of electronic transitions in a variety of glasses.[35]

Figure 4 demonstrates that the underlying temperature dependence of the vibrational homogeneous dephasing measured with the IR photon echoes is, in fact, identical in the three glasses studied here and is described by a power law T^2. The results presented here were the first to examine the temperature dependence of vibrational dephasing in organic glasses.[7-9,15] The observation of the T^2 dependence suggests that these glasses are in the high-temperature limit above 10 K and that the temperature dependence of vibrational pure dephasing may be universal in all high-temperature glasses. This would be consistent with dephasing caused by Raman (two quantum) phonon scattering.

2. Above the Glass Transition Temperature. The temperature dependences of the rate of dephasing in 2-MP and 2-MTHF (Figure 3) both show a gradual increase with temperature until shortly after the glass transition, at which point a rapid increase in dephasing is observed. Coincidentally, the glass transition temperatures for 2-MP ($T_g = 80$ K) and 2-MTHF ($T_g = 86$ K) are very similar. The temperature dependence in DBP shows no dramatic change near 90 K, demonstrating that the mechanism is dependent on the solvent; the dephasing is dictated by the particular temperature-dependent dynamics of the solvent. At temperatures above the glass transition, the normalized line widths in the three liquids diverge from each other, indicating the emergence of distinct relaxation processes in the various liquids.[15]

In 2-MTHF and in 2-MP below 150 K, the echo decays yield a homogeneous line width that is much narrower than the width of the absorption spectrum. These results demonstrate that the vibrational lines of these systems are inhomogeneously broadened in the glass and supercooled liquid. As shown below, in 2-MP the $W(CO)_6$ T_{1u} line becomes homogeneously broadened at room temperature. However, in DBP the line is clearly inhomogeneous at all temperatures. The homogeneous line width at 300 K is ~1 cm^{-1}, while the absorption spectrum line

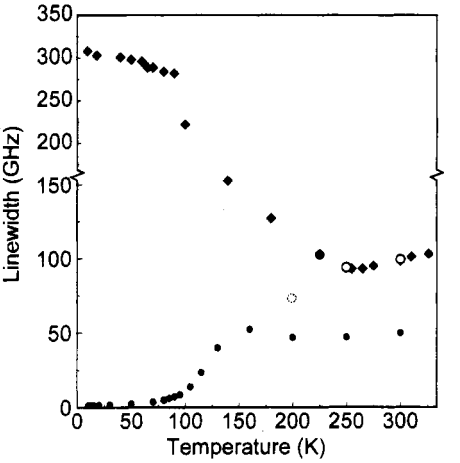

Figure 5. Temperature dependence of the homogeneous and absorption line widths for the T_{1u} mode of $W(CO)_6$ in 2-MP. The homogeneous line widths (solid circles) are taken from Figure 4. The "echo" data at 250 and 300 K are actually free induction decays that match the observed absorption line (open circles), showing the spectra are homogeneously broadened. At 200 K (dotted circle), the homogeneous and inhomogeneous contributions to the absorption line are of equal magnitude. Below 200 K, the homogeneous line width is much narrower than the inhomogeneous width.

width is 26 cm^{-1}. This is the first conclusive evidence for intrinsic inhomogeneous broadening of a vibrational line in a room temperature liquid. Thus, even in room temperature liquids, it is not safe to assume that dynamics can be obtained by taking a vibrational spectrum and analyzing it assuming it is homogeneously broadened.

C. Contributions to the Homogeneous Line Shape in 2-MP. *1. Transition to a Homogeneously Broadened Line.* The measured homogeneous vibrational line width obtained from infrared photon echo measurements (Figure 3) assumed that the echo decays as eq 9b. This equation is valid in the inhomogeneous limit, when the width of the inhomogeneous distribution of homogeneous lines far exceeds the homogeneous line width. This inhomogeneous limit implies a separation of time scales exists between the fast fluctuations of homogeneous dephasing and long time-scale inhomogeneous structural evolution. Such is the case below 150 K, where the echo decays yield a homogeneous line width that is much narrower than the width of the absorption spectrum. At these temperatures, the data demonstrate with certainty that the T_{1u} vibrational line in 2-MP is substantially inhomogeneously broadened.

Above 150 K, the homogeneous line width begins to approach the measured absorption line width,[14,15] as illustrated in Figure 5. Under these conditions, the time scale for the rephasing of the echo pulse is shortened by the polarization decay due to homogeneous dephasing. This causes the echo to rephase at times between τ and 2τ. Thus, the echo signal decays at a slower rate than the $4/T_2$ given by eq 9b.[39,40] As the homogeneous dephasing time T_2 decreases, the rephasing of the echo is shifted to shorter times. In the limit that the absorption line is homogeneously broadened, a free induction decay (fid) will be observed along the echo phase matching direction. If the homogeneous line is a Lorentzian, then an exponential decay with a decay constant of $2/T_2$ will be observed.[40]

The data above 150 K reflect this transition to a homogeneously broadened line. If near room temperature the measured echo data are actually fid's from a homogeneously broadened line, the decay constants $2/T_2$ yield a line width given by the open circles in Figure 5. The FID line widths match the measured absorption line widths exactly, demonstrating that the line is homogeneously broadened for temperatures ≥250 K.

Notice that the absorption line width, which narrows for temperatures up to 200 K, actually broadens slightly for higher temperatures, in a manner that precisely follows the echo data. Without experimentally time-resolving the rephasing of the echo pulse, it is not possible to determine from an echo experiment alone whether the observable is a true echo decay, a fid, or an intermediate case. However, a comparison to the absorption spectrum provides a test. Since treating the point at 160 K as an fid still results in a line width that is narrower than the absorption line, this point corresponds to a true photon echo. The point at 200 K represents the transition between a homogeneous and an inhomogeneous absorption line shape.

In liquids, the distinction between homogeneous and inhomogeneous broadening is a matter of definitions and time scales. A photon echo experiment measures the homogeneous line shape, which arises from fast fluctuations of the medium that cause rapid fluctuations of the vibrational energy levels. In a liquid, the homogeneous line width can be much narrower than the inhomogeneous line width even at room temperature, as shown above for $W(CO)_6$ in DBP. The slower dynamic processes, which are essentially static on the time scale of the homogeneous dephasing, appear as part of the quasi-static inhomogeneous background. This quasi-static distribution of vibrational energies is rephased in a photon echo experiment and does not contribute to the homogeneous line width.

2. Components of the Homogeneous Line. Pump−probe studies of the population dynamics of the T_{1u} mode of $W(CO)_6$ in 2-MP have observed dynamics that contribute to the infrared absorption line shape.[14,15] In addition to pure dephasing (energy fluctuations), population relaxation and orientational relaxation contribute to the homogeneous line width. Pump−probe measurements of the population dynamics in 2-MP and other solvents were performed.[14,15,17] A detailed analysis of the population dynamics and their temperature dependences for the 2-MP data is given in ref 14. The data taken with parallel pump and probe polarizations are biexponential at all temperatures. The long decay component is due to vibrational population relaxation (lifetime) and decays with an exponential decay time of T_1. The data display a counterintuitive temperature dependence, with the rate of relaxation decreasing as the temperature increases. This phenomenon has also been observed in crystallizing and other glass-forming liquids[15,17] and is discussed in some detail below.[16] The fast component in the pump−probe data is due to orientational relaxation of the chromophore and decays exponentially at a rate of $(6D_{or} + 1/T_1)$. With magic angle probing to eliminate orientational relaxation effects, the fast component vanished from the decay, leaving only the long component.

Equation 9 gives a Lorentzian line shape, and contributions to the full line width at half-maximum are additive, given in eqs 4 and 5. Using the pump−probe measurements of the orientational diffusion constant D_{or} and the population relaxation time T_1,[14,15] the contribution due to pure dephasing can be determined from the homogeneous line width. (There are a number of subtle issues involved in considering the influence of orientational relaxation on the photon echo decay. A full discussion of these in relation to the material presented below is given in ref 15.)

Figure 6 displays the decomposition of the temperature dependence of the homogeneous vibrational line width into its three dynamic components.[15] At low temperatures, the lifetime is the dominate contribution. At high temperatures, pure dephasing is the dominate contribution. Only at intermediate temperatures does orientational relaxation make a substantial contribution. The line width contribution from lifetime broadening remains significant until ~50 K. Above 50 K, the contributions to the line width from pure dephasing and orientational relaxation dominate. Orientational relaxation does not dominate in any temperature range but makes its largest percentage contribution around 100 K. By 100 K, the pure dephasing is a substantially larger contribution than either the lifetime or the orientational relaxation. Above ~150 K, pure dephasing is the overwhelmingly dominate component of the homogeneous line width.

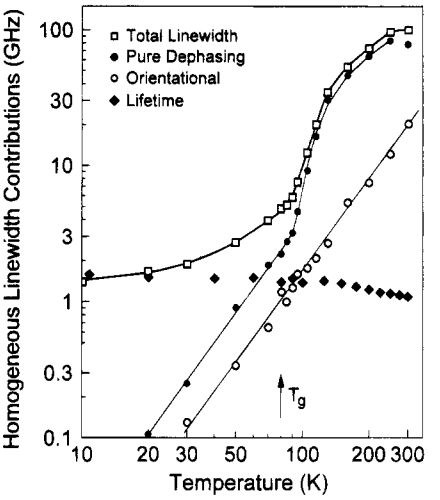

Figure 6. A log−log plot of the dynamic contributions to the homogeneous vibrational line width of the T_{1u} mode of $W(CO)_6$ in 2-MP: total line width, squares; lifetime contribution, diamonds; pure dephasing contribution, solid circles; orientational contribution, open circles. The vibrational lifetime dominates the homogeneous line width at the lowest temperatures and is only mildly temperature dependent. At high temperatures, pure dephasing dominates the homogeneous line width. Orientational relaxation never dominates but makes significant contributions to the line width at intermediate temperatures. The orientational contribution, shown with a T^2 power law line, is continuous over all temperatures. The temperature dependence of the pure dephasing is the same as the orientational relaxation in the glass. The line through the pure dephasing data is a fit to eq 13 with $\alpha = 2.2$ and $T_0^* = 80$ K. Error bars on the total line width, lifetime, and pure dephasing are approximately the size of the symbols at most temperatures. The orientational error bars vary from the size of the symbols at high temperature to ±50% at 30 K.

At low temperature, where the contributions from pure dephasing and orientational relaxation are negligible, the contribution to the line width from the lifetime (from pump−probe data) and the line width determined from the decay of the echo are equal within error. This is the expected low-temperature limit for the homogeneous vibrational line width where processes caused by thermal fluctuations disappear, and only lifetime broadening is possible.

From low temperature to slightly above T_g, both pure dephasing and orientational relaxation have power law temperature dependences. The earlier discussion of the combined dynamics in 2-MP and the other two solvents showed a T^2 temperature dependence when the lifetime contribution was taken out. Here, the contributions from both pure dephasing and orientational relaxation are shown to follow the same T^2 power law behavior in the glass. Thus, the total temperature dependence, excluding T_1, is T^2, as shown in Figure 4. In addition, the power law observed for the orientational relaxation in the glass is observed to continue into the liquid. In Figure 6, a power law fit of $\alpha = 2.2 \pm 0.2$ is shown. The orientational dynamics are independent of the glass transition and distinctly nonhydrodynamic.[15] This is consistent with the results of pump−probe experiments.[14]

In Figure 6 it is seen that there is a rapid increase in pure dephasing beginning slightly above the glass transition temperature. This implies that an additional mechanism or a change in the nature of the mechanism for pure dephasing turns on, and it is linked to the glass-to-liquid transition. The onset of dynamic processes near the glass transition is often described with a Vogel–Tammann–Fulcher (VTF) equation[41-43]

$$\tau = \tau_0 \exp(B/(T - T_0)) \qquad (12)$$

This equation describes a process characterized by a time, τ, with a temperature-dependent activation energy that diverges at a temperature, T_0, below the nominal glass transition temperature. T_0 can be linked thermodynamically to an "ideal" glass transition temperature that would be measured with an ergodic observable.[41] This equation describes the temperature dependence of the viscosity of 2-MP well and gives $T_0 = 59$ K.[15]

If the VTF equation applies to pure dephasing near and above the glass transition, then the full temperature dependence would be the sum of the low-temperature power law plus a VTF term. To test this idea, the temperature dependence of pure dephasing was fit to

$$\Gamma^*(T) = A_1 T^{\alpha} + A_2 \exp(-B/(T - T_0^*)) \qquad (13)$$

for all temperatures below 300 K, and is shown as the line through the pure dephasing data in Figure 6. The fit describes the entire temperature dependence exceedingly well but yields a reference temperature of $T_0^* = 80$ K. This reference temperature matches the laboratory glass transition temperature T_g exactly but is not related to the ideal glass transition temperature T_0. We can thus infer that the onset of the dynamics that cause the rapid increase in homogeneous dephasing in 2-MP is closely linked with the onset of structural processes near the laboratory glass transition temperature. This may be a manifestation of the short time scale of the measurement and a reflection of the nonergodicity of the system.

D. Vibrational Lifetimes Measured with IR Pump–Probe Experiments. The population dynamics of the vibrations of a polyatomic solute molecule in a polyatomic solvent can involve the internal vibrational modes of the solute, the vibrational modes of the solvent, and the low-frequency continuum of solvent modes.[17,18] An initially excited high-frequency vibrational mode of a solute molecule can relax by transferring vibrational energy to a combination of lower frequency internal vibrations and solvent vibrations. Vibrational energy can also be transferred to modes of higher frequency, but this process is generally less efficient than comparable downward pathways.[18] In general, a combination of lower frequency vibrations will not match the initial vibrational frequency. Therefore, one or more quanta of the continuum will also be excited (or annihilated) to make up for the mismatch in the vibrational frequencies and conserve energy. The low-frequency solvent continuum can be described in terms of instantaneous normal modes (INM).[44-48] Not all of the modes are bound, so that INM's have both real and imaginary frequencies. The imaginary frequency modes are related to the structural evolution of the liquid.[49]

Vibrational relaxation involves a cubic or higher order anharmonic process. The "order" of the process refers to the number of quanta involved in the relaxation. In the simplest cubic anharmonic process, the initial excited vibration is annihilated, a lower frequency internal mode or solvent mode is excited, and a phonon (INM) is excited to conserve energy. For a high-frequency mode to relax by a cubic process, there must be another high-frequency mode close enough in energy for the energy mismatch to fall within the phonon bandwidth. In a quartic or higher order process, the initial vibration is annihilated, two or more lower frequency vibrations are created, and one or more phonons are created to conserve energy. Unless there is a coincidence or Fermi resonance in which energy can be conserved by the creation and annihilation of discrete vibrational modes alone, at least one mode of the low-frequency continuum of states will be involved in vibrational population dynamics.

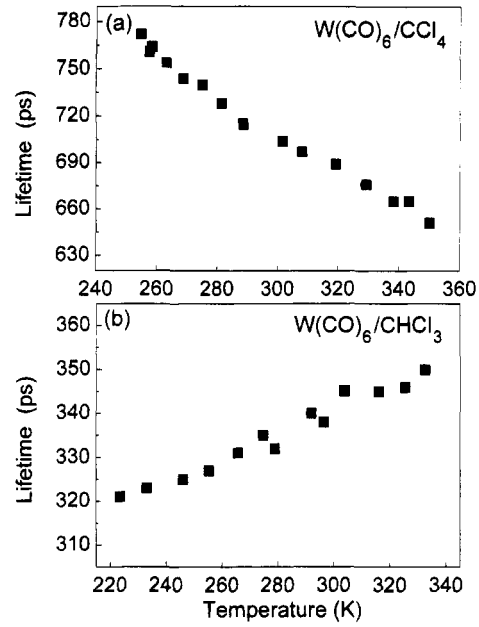

Figure 7. (a) Temperature dependence of the vibrational relaxation time, T_1, for the T_{1u} CO stretching mode of $W(CO)_6$ in CCl_4. The data were taken from the melting point to the boiling point. (b) Temperature dependence of T_1 in $CHCl_3$. The data were taken from the melting point to the boiling point. The lifetime actually becomes slower as the temperature is increased (inverted temperature dependence).

The vibrational relaxation times (T_1) as a function of temperature for T_{1u} mode of $W(CO)_6$ in CCl_4[17] are shown in Figure 7a. Although the change in the decay with temperature is not large, given the excellent signal-to-noise ratio of the data,[17] the differences are readily discernible. From the melting point to the boiling point, the lifetimes decrease monotonically by 19%. The values range from 775 ps at the melting point (250 K) to 650 ps at the boiling point (350 K).

The results of the pump–probe lifetime measurements in $CHCl_3$[17] are shown in Figure 7b. The decay times are substantially different from those in CCl_4 although the solvents differ only by substitution of a hydrogen for a chlorine. Even more significant is that the basic nature of the temperature dependence is different. Vibrational lifetimes for the T_{1u} mode of $W(CO)_6$/$CHCl_3$ actually become *longer as the temperature is increased*, changing by 9% from 322 ps at the melting point (210 K) to 350 ps at the boiling point (334 K). This is analogous to the temperature dependence of T_1 seen in 2-MP (see Figure 6).

$W(CO)_6$ has a variety of internal modes that are lower in frequency than the initially excited T_{1u} CO stretching frequency.[16,17] Both CCl_4 and $CHCl_3$ have a number of lower energy vibrational modes than the initially excited mode at ~1980 cm^{-1}.[16,17] $CHCl_3$ also has a CH stretching mode at higher energy, ~3020 cm^{-1}, which is too high in energy to participate in the vibrational dynamics. The simplest relaxation pathway would involve the deposition of the initial vibrational energy into a single lower frequency vibration and one phonon.

However, as shown by INM calculations, neither CCl_4 nor $CHCl_3$ has INM bandwidths that extend past 180 cm^{-1}.[16] Therefore, in $CHCl_3$, it is necessary for the initial vibration to relax into at least two vibrations and a phonon and in CCl_4 to relax into at least three vibrations and a phonon. This difference most likely is responsible for the generally longer relaxation times observed in CCl_4. It is possible that it is necessary to excite more than one phonon to conserve energy. For simplicity, the following discussion assumes that only one phonon is involved, although this will not influence the conclusions that are reached.

The rate of vibrational relaxation, K, of the initially excited mode is generally described by Fermi's Golden Rule[18,26,50]

$$K = (2\pi/\hbar)\sum_{r,r'} \varrho_{r,r'} |\langle \sigma',r'|V|\sigma,r\rangle|^2 \qquad (14)$$

In eq 14, σ and σ' denote the initial and final state of the initially excited vibration (the T_{1u} mode in this case), while r and r′ refer to the receiving (or reservoir) modes. The ket $|\sigma,r\rangle$ is the initial state, described by thermal occupation numbers of the various modes of the system, in addition to unit occupation of the state initially excited by the IR pump. The bra $\langle\sigma',r'|$ is the final state with the initially populated state having occupation number 0 after relaxation and other states having increased occupation numbers. ϱ is the density of states of the reservoir modes for the relaxation step and is often written as a delta function to denote the energy conservation requirement. The summation in eq 14 denotes the fact that the true relaxation rate is a sum over contributions from all possible pathways;[18] however, in the following discussion we will describe relaxation through a single anharmonic path involving one phonon.

In eq 14, V is the potential that describes the system−reservoir interaction.[18] The potential energy surface for the system and reservoir is expanded about the potential minima of the various INM coordinates. $V^{(i)}$ is the ith matrix element that describes the interactions which couple i modes. The anharmonic terms, $i \geq 3$, govern relaxation processes involving the coupling of multiple vibrational modes. The magnitudes of the matrix element expansion coefficients decrease with order, leading to decreased relaxation rates with higher order processes.

Given the vibrational energies of the solutes and the solvents, the relaxation of the initially excited mode results in the excitation of at least two other vibrations and a phonon. For such a process, the anharmonic coupling matrix element is at least fourth order, or quartic. For the following discussion, we use one of the quartic relaxation paths that contributes to the relaxation of the T_{1u} CO stretch in $CHCl_3$.[16] The CO stretch relaxes by transferring energy to the W−C−O bending motion of the $W(CO)_6$, the H−C−Cl bending motion of the $CHCl_3$, and a ~160 cm^{-1} solvent phonon.

The quartic anharmonic matrix element $\langle V^{(4)}\rangle$ contains the magnitude of the quartic anharmonic coupling term, $|V^{(4)}|$, and combinations of raising and lowering operators that describe the anharmonic relaxation step.[17,18] If the operator a annihilates the initially excited vibration and the operator b describes the change in the reservoir modes A, B, and the phonon, then the interaction is described by

$$a(b_A + b_A^+)(b_B + b_B^+)(b_{ph} + b_{ph}^+) \qquad (15)$$

This interaction leads to seven possible quartic relaxation pathways,[18] some of which are unphysical. The relaxation pathway being considered, a simple cascade process in which the energy relaxes only to lower energy modes, is described by one term arising from eq 15, $ab_A^+b_B^+b_{ph}^+$. Once substituted into eq 14, a raising operator brings out a factor of $\sqrt{n+1}$ and a lowering operator brings out a factor of $\sqrt{n}$, where n is the occupation number of the particular mode involved in the fourth-order process. This allows eq 14 to be written as

$$K = (2\pi/\hbar)\varrho_{ph}|\langle V^{(4)}\rangle|^2 (n_A + 1)(n_B + 1)(n_{ph} + 1) \qquad (16)$$

where n is the thermally averaged occupation number,

$$n_i = (\exp(\hbar\omega_i/kT) - 1)^{-1} \qquad (17)$$

ω_i is the frequency of the vibrational or phonon mode. We take $\varrho_{ph} = \langle\varrho(\omega_i)\rangle$; i.e., the "phonon" density of states is given by the ensemble-averaged density of INM.

Clearly, if the reservoir modes are high frequency ($\hbar\omega \gg kT$ and, therefore, $n \ll 1$), such as the discrete vibrational modes of the solute and solvent, eq 16 is

$$K = (2\pi/\hbar)\varrho_{ph}|\langle V^{(4)}\rangle|^2 (n_{ph} + 1) \qquad (18)$$

Although the discussion of the derivation of this relaxation rate expression has been qualitative, the same results can be shown rigorously.[18] In general, the expression for the relaxation rate along a given one-phonon, ith-order anharmonic pathway is given by the product of the phonon density of states, the magnitude of the anharmonic coupling matrix element squared, and occupation number factors for the receiving modes. If a reservoir mode is created in the relaxation step, it contributes a factor of $(n + 1)$, whereas if it is annihilated, it contributes a factor of n. This is a simple, yet rigorous, method for describing even complex relaxation pathways.

Considering only the occupation number in eq 18, K should become larger, and the observed decay times should become shorter as the temperature is increased. If more than one thermally occupied phonon were involved in the relaxation pathway or if a vibrational occupation number changes significantly, the temperature dependence would be even steeper. If the phonon occupation number is the only factor responsible for the temperature dependence, then for $\hbar\omega \ll kT$, K would increase linearly with temperature. For $\hbar\omega \gg kT$, K goes as $\exp(-\hbar\omega/kT)$ if a phonon is annihilated as part of the relaxation process, and K goes as $1 + \exp(-\hbar\omega/kT)$ if a phonon is created. In either limit and for intermediate situations, the temperature dependence of the occupation number(s) will always yield a decrease in the vibrational lifetime with increasing temperature. Only near $T \approx 0$ K (only phonon emission processes are possible) where $1 > n_{ph}$ will the temperature dependence vanish, and the vibrational lifetime will become temperature independent. Above $T \approx 0$ K, an inverted temperature dependence cannot be explained by considering occupation numbers, regardless of the pathways or number of modes involved.[18]

The experimental data for $W(CO)_6$ in $CHCl_3$ displayed in Figure 7b, with its inverted temperature dependence, show that the temperature dependence is influenced by temperature-dependent factors in addition to the occupation numbers. A competition among these factors will yield the observed temperature dependence.[16,17] The factors that cause the $W(CO)_6$/$CHCl_3$ vibrational lifetimes to become longer as the temperature is increased are operative in $W(CO)_6$ in CCl_4 and presumably other systems, even though they do display vibrational lifetimes that decrease with increasing temperature.[16]

In examining eq 16 or 18, there are two other factors besides the occupation numbers that can contribute to the temperature dependence of the decay constant. They are the density of states, ϱ, and the magnitude of the anharmonic coupling matrix element, $V^{(i)}$. First, consider the density of states.[16,17] The

densities of states of the internal vibrational modes of $W(CO)_6$ do not change with temperature. However, the densities of states of the solvent modes will change with temperature.

To gain insights into the temperature dependences of the vibrational lifetimes in the two solvents, the temperature-dependent low-frequency INM spectra, $\langle\rho(\omega)\rangle$, of CCl_4 and $CHCl_3$ were calculated.[16] The calculations employed a detailed potential that included intermolecular and intramolecular components. While the low-frequency intermolecular modes are of interest here, the potential is able to do a reasonable job of reproducing the vibrational spectrum of the liquids as well. The use of the full potential proved important. Calculations with an accurate Lennard-Jones (LJ) potential do not generate the high-frequency "rotational" part of the INM spectrum even though the LJ potential yields the correct melting point of the crystal. The real and imaginary components of the INM spectrum were calculated at three temperatures: near the melting point, at room temperature, and near the boiling point for both solvents. As the temperature is increased, there is a small decrease in the density of states across most of the real part of the spectra with a corresponding increase in the imaginary part. The changes in the two solvents were very similar, and detailed analysis[16] showed that the changes were far too small to account for the observed inverted temperature dependence.

These results suggest that a significant temperature dependence exists for the magnitude $V^{(i)}$. The temperature dependence of this term must be opposite to that of the phonon occupation numbers and must be sufficiently large to offset the change in occupation numbers to yield the inverted temperature dependence. Although $V^{(i)}$ is not explicitly temperature dependent, it can vary with density. As the density decreases with increasing temperature, intermolecular separations are increased on average. The important point is that the region of the intermolecular potential that is sampled changes, and therefore the anharmonic coupling matrix elements can change. If this causes the matrix elements to become smaller with increasing temperature, then this decrease will work to offset the increase in occupation numbers. If this effect is sufficiently large, the observed inverted temperature dependence of $W(CO)_6/CHCl_3$ would be observed. This is the most likely explanation for the inverted temperature dependence.

Three factors were discussed that will influence the vibrational lifetime of the metal carbonyls studied and, presumably, other systems as well. They are (1) the temperature-dependent occupation number of the phonon(s) or other very low-frequency modes excited in the relaxation of the initially pumped vibration, (2) the temperature dependence of the liquid's density of INM states, and (3) the temperature dependence of the magnitude of the anharmonic coupling matrix elements responsible for vibrational relaxation. The results briefly discussed here demonstrate that understanding the temperature dependence of vibrational lifetimes requires consideration of the interplay of the temperature dependences of the three factors. Observation of a normal (noninverted) temperature dependence does not indicate that all three factors are not involved. Fitting a normal temperature dependence as a simple activated process can yield a highly flawed indication of the frequency of the low-frequency mode that is involved.

IV. Concluding Remarks

In principle, analysis of a vibrational line shape can provide a great deal of information on dynamics and intermolecular interactions in condensed matter systems. However, to completely characterize an infrared line shape, a combination of experimental methods is necessary to elucidate each of the dynamic and static contributions to the line. Picosecond infrared photon echo experiments were used to measure the homogeneous line shape and remove inhomogeneity. Infrared pump–probe experiments were used to measure the vibrational lifetime and orientational relaxation. The total vibrational line shape was determined by absorption spectroscopy. Together, these experiments yield a complete characterization of the dynamics that make up the homogeneous line and the extent of inhomogeneity of the infrared absorption line.

The development of picosecond vibrational photon echo experiments to examine condensed matter systems represents a significant extension of the field of vibrational spectroscopy. Recently, we have also applied other IR nonlinear experimental methods to study vibrations. We have used stimulated photon echoes and transient grating experiments. All of these methods are types of four-wave mixing experiments. The application of four-wave mixing experiments to the study of electronic states and nonresonant phenomena in the visible part of the spectrum has had explosive growth in the 1980s and 1990s. Vibrational spectroscopy has always gained importance because of its selectivity, i.e., its ability to look at specific, well-defined mechanical degrees of freedom of molecules. The advent of IR vibrational four-wave mixing experiments, such as the photon echo experiments described here, will provide important tools to greatly increase our understanding of the dynamics and intermolecular interactions in molecular systems of interest in chemistry, biology, and materials science.

Acknowledgment. The authors thank Professor Alan Schwettman and Professor Todd Smith of the Department of Physics, Stanford University, and their groups for the opportunity to use the Stanford Free Electron Laser. This work was supported by the National Science Foundation (DMR93-22504), the Office of Naval Research (N00014-92-J-1227), the Medical Free Electron Laser Program (N00014-91-C-0170), and the Air Force Office of Scientific Research (F49620-94-1-0141).

References and Notes

(1) Gordon, R. G. *J. Chem. Phys.* **1965**, *43*, 1307.
(2) Gordon, R. G. *Adv. Magn. Reson.* **1968**, *3*, 1.
(3) Berne, B. J. In *Physical Chemistry: An Advanced Treatise*; Henderson, D., Ed.; Academic Press: New York, 1971; Vol. VIIIB.
(4) Yarwood, J. *Annu. Rep. Prog. Chem., Sect. C* **1979**, *76*, 99.
(5) Rothschild, W. G. *Dynamics of Molecular Liquids*; John Wiley and Sons: New York, 1984.
(6) Loring, R. F.; Mukamel, S. *J. Chem. Phys.* **1985**, *83*, 2116.
(7) Zimdars, D.; Tokmakoff, A.; Chen, S.; Greenfield, S. R.; Fayer, M. D. *Phys. Rev. Lett.* **1993**, *70*, 2718.
(8) Tokmakoff, A.; Zimdars, D.; Sauter, B.; Francis, R. S.; Kwok, A. S.; Fayer, M. D. *J. Chem. Phys.* **1994**, *101*, 1741.
(9) Tokmakoff, A.; Kwok, A. S.; Urdahl, R. S.; Francis, R. S.; Fayer, M. D. *Chem. Phys. Lett.* **1995**, *234*, 289.
(10) Vanden Bout, D.; Muller, L. J.; Berg, M. *Phys. Rev. Lett.* **1991**, *67*, 3700.
(11) Muller, L. J.; Vanden Bout, D.; Berg, M. *J. Chem. Phys.* **1993**, *99*, 810.
(12) Inaba, R.; Tominaga, K.; Tasumi, M.; Nelson, K. A.; Yoshihara, K. *Chem. Phys. Lett.* **1993**, *211*, 183.
(13) Vanden Bout, D.; Freitas, J. E.; Berg, M. *Chem. Phys. Lett.* **1994**, *229*, 87.
(14) Tokmakoff, A.; Urdahl, R. S.; Zimdars, D.; Kwok, A. S.; Francis, R. S.; Fayer, M. D. *J. Chem. Phys.* **1995**, *102*, 3919.
(15) Tokmakoff, A.; Fayer, M. D. *J. Chem. Phys.*, in press.
(16) Moore, P.; Tokmakoff, A.; Keyes, T.; Fayer, M. D. *J. Chem. Phys.*, in press.
(17) Tokmakoff, A.; Sauter, B.; Fayer, M. D. *J. Chem. Phys.* **1994**, *100*, 9035.
(18) Kenkre, V. M.; Tokmakoff, A.; Fayer, M. D. *J. Chem. Phys.* **1994**, *101*, 10618.
(19) Hahn, E. L. *Phys. Rev.* **1950**, *80*, 580.
(20) Kurnit, N. A.; Abella, I. D.; Hartmann, S. R. *Phys. Rev. Lett.* **1964**, *13*, 567. Abella, I. D.; Kurnit, N. A.; Hartmann, S. R. *Phys. Rev.* **1966**, *141*, 391.

(21) Farrar, T. C.; Becker, D. E. *Pulse and Fourier Transform NMR*; Academic Press: New York, 1971. Skinner, J. L.; Andersen, H. C.; Fayer, M. D. *J. Chem. Phys.* **1981**, *75*, 3195.
(22) Chesnoy, J.; Gale, G. M. *Adv. Chem. Phys.* **1988**, *70*, 297.
(23) Califano, S.; Schettino, V.; Neto, N. *Lattice Dynamics of Molecular Crystals*; Springer-Verlag: Berlin, 1981.
(24) Velsko, S.; Hochstrasser, R. M. *J. Phys. Chem.* **1985**, *89*, 2240.
(25) Schweizer, K. S.; Chandler, D. *J. Chem. Phys.* **1982**, *76*, 2296.
(26) Oxtoby, D. W. *Annu. Rev. Phys. Chem.* **1981**, *32*, 77.
(27) Narasimhan, L. R.; Littau, K. A.; Pack, D. W.; Bai, Y. S.; Elschner, A.; Fayer, M. D. *Chem. Rev.* **1990**, *90*, 439.
(28) Berne, B. J.; Pecora, R. *Dyanmic Light Scattering*; R. E. Krieger Publishing: Malabar, FL, 1990.
(29) Bratos, S.; Leicknam, J. C. *J. Chem. Phys.* **1994**, *101*, 4536.
(30) Mukamel, S.; Loring, R. F. *J. Opt. Soc. B* **1986**, *3*, 595.
(31) Loring, R. F.; Mukamel, S. *Chem. Phys. Lett.* **1985**, *114*, 426.
(32) Tokmakoff, A.; Marshall, C. D.; Fayer, M. D. *J.O.S.A. B* **1993**, *10*, 1785.
(33) Yan, Y. J.; Mukamel, S. *J. Chem. Phys.* **1991**, *94*, 179.
(34) Arrivo, S. M.; Dougherty, T. P.; Grubbs, W. t.; Heilweil, E. J. *Chem. Phys. Lett.* **1995**, *235*, 247.
(35) Macfarlane, R. M.; Shelby, R. M. *J. Lumin.* **1987**, *36*, 179.
(36) Anderson, P. W.; Halperin, B. I.; Varma, C. M. *Philos. Mag.* **1972**, *25*, 1.
(37) Phillips, W. A. *J. Low Temp. Phys.* **1972**, *7*, 351.
(38) Huber, D. L. *J. Non-Cryst. Solids* **1982**, *51*, 241.
(39) Cho, M.; Fleming, G. R. *J. Chem. Phys.* **1993**, *98*, 2848.
(40) Joo, T.; Albrecht, A. C. *Chem. Phys.* **1993**, *176*, 233.
(41) Angell, C. A. *J. Phys. Chem. Solids* **1988**, *49*, 863.
(42) Angell, C. A. *J. Phys. Chem.* **1982**, *86*, 3845.
(43) Fredrickson, G. H. *Annu. Rev. Phys. Chem.* **1988**, *39*, 149.
(44) Seeley, G.; Keyes, T. *J. Chem. Phys.* **1989**, *91*, 5581.
(45) Xu, B. C.; Stratt, R. M. *J. Chem. Phys.* **1990**, *92*, 1923.
(46) Wu, T. M.; Loring, R. M. *J. Chem. Phys.* **1992**, *97*, 8568.
(47) Moore, P.; Keyes, T. *J. Chem. Phys.* **1993**, *100*, 6709.
(48) Cho, M.; Fleming, G. R.; Saito, S.; Ohmine, I.; Stratt, R. M. *J. Chem. Phys.* **1994**, *100*, 6672.
(49) Keyes, T. *J. Chem. Phys.* **1994**, *101*, 5081.
(50) Oxtoby, D. W. *Adv. Chem. Phys.* **1981**, *47*, 487.

JP951323Y